Rotor Hover Performance and Flowfield Measurements with Untwisted and Highly-twisted Blades

Manikandan Ramasamy*
University Affiliated Research Center
NASA Ames Research Center
Moffett Field, CA 94035

Nili P. Gold† and Mahendra J. Bhagwat‡
Aeroflightdynamics Directorate
U. S. Army Research, Development, and Engineering Command (*AMRDEC*)
Moffett Field, CA 94035

Abstract

The flowfield and performance characteristics of highly-twisted blades were analyzed at various thrust conditions. Similar measurements made using untwisted blades helped understand the effect of high twist on the wake structure and, in turn, on rotor performance. Twisted blades are known to give better hover performance than untwisted blades at high thrust coefficients (because of the more uniform inflow and the associated reduction in induced power) typical of those found in full-scale rotors. However, the present experiments were conducted at sufficiently low thrust (beginning from zero thrust), where the untwisted blades showed identical, if not better, performance when compared with the highly-twisted blades. The flowfield measurements showed some key wake differences between the two rotors. These observations combined with simple blade element momentum theory (also called annular disk momentum theory), helped understand the induced power requirements and, thereby, rotor performance characteristics.

Nomenclature

A	rotor disk area, m^2
A	Radial contraction ratio
B,C,m,n	Kocurek-Tangler model parameters
C_Q	Rotor torque coefficient
C_T	Rotor thrust coefficient
k_1	Axial convection rate until 1^{st} blade passage
k_2	Axial convection rate after 1^{st} blade passage
N_b	Number of blades
r	Radial distance, m
R	Rotor radius, m
V	Vertical (axial) velocity ms^{-1}
z	Axial distance, m
Γ	Blade bound circulation, m^2s^{-1}
γ	Radial contraction rate parameter
θ_{tw}	Linear twist rate
λ	Inflow ratio, $=V/V_{\text{tip}}$
λ_h	Ideal induced inflow ratio, $=\sqrt{C_T/2}$
ψ	Rotor azimuth, deg
ψ_w	Wake azimuth, deg

*Research Scientist. **mani.ramasamy@us.army.mil**
†Research Scientist. **nili.p.gold@us.army.mil**
‡Research Scientist. **mahendra.bhagwat@us.army.mil**
Presented at the 36th European Rotorcraft Forum, Paris, France, September 7–9, 2010.

Introduction

U. S. Army's interest in developing heavy-lift helicopters, combined with NASA's interest in developing large civil tilt-rotors reinvigorated aerodynamic research on highly-twisted blades. Any improvement in the efficiency/capability of a rotor system should stem from improving the understanding of rotor wakes and their influence on the overall rotor performance. The time evolution of the wake structure is a fundamental factor influencing the performance of a rotor system. This is understandable considering that the rotor operates in close vicinity of its own wake in hover with large consequences for induced power. Over the past several decades, significant efforts have been spent towards analyzing rotor wakes – both experimentally and computationally (Refs. 1–5). Although the gross features of the rotor wake and their influence on power are known, many smaller, but consequential, details are not clearly understood. Yet, such small details may be crucial to designers who are looking for small improvements in hover performance (of the order of one percent or smaller in figure of merit). Because such a level of accuracy may not be feasible with either measurements or predictions, it is necessary to understand the underlying physics with more detailed wake flow field measurements.

A overview of the existing literature suggests that more often than not, experimental studies have been limited to the blade tip region (Refs. 6–13). This is because majority of the thrust is produced on the outboard sections

of the blade. Also, the tip vortices are the most dominant flow structures in the rotor wake. However, other aspects of the wake structure can also be significant and can provide insight into the rotor flow physics. For example, the wake sheet geometry reflects the spanwise inflow distribution and this can vary significantly with thrust. Root vortices are also sometimes observed in the rotor wake but are more difficult to visualize because of the higher levels of turbulence found in this region. Both these can be significantly different between different rotor designs. Modern computational fluid dynamics (CFD) solutions using large grids can compute many of these features. Thanks to the advances in high-speed computation, CFD methods for rotor applications continue to gain momentum and have resulted in reasonable success in terms of performance prediction. Currently, more detailed experimental studies are needed to compliment these CFD advances and to provide greater physical understanding.

Experimental measurements of rotor wake structure are the foundations of prescribed wake models that are often used in performance analyses as well as in design. These are based on rotor wake flow visualization studies using several rotor configurations with untwisted and linearly twisted blades. These models relate wake geometry to rotor parameters like thrust, solidity, blade twist, etc. The Landgrebe model (Ref. 2) includes inboard vortex sheet geometry described as a linear sheet connecting its inner and outer edges. Root vortices tend to be neglected, perhaps because for untwisted blades the root vortex would have negligible strength, similar to moderately twisted blades. Other prescribed wake models, e.g., the Kocurek-Tangler model (Ref. 14), included more blade geometric parameters, but modeled only the tip vortices. Flow visualization studies of a model UH-60 rotor in hover quantified inner wake sheet locations and its evolution with increasing thrust (Ref. 15). However, in most of the open literature the inboard wake sheet has not been studied in as much detail as the tip vortices. One objective of the present work is to identify the inboard wake structures and to relate these to performance.

Performance and flow field measurements were acquired on a model scale helicopter rotor using untwisted and highly-twisted blades. Contrary to expectations, the highly-twisted blades did not show significant difference in performance compared to the untwisted blades. However, the flow field measurements showed key differences in the wake structure which helped to understand this performance behavior. The paper documents the time-averaged velocity distribution in the rotor wake, which together with blade element momentum theory explains the performance differences between highly-twisted and untwisted blades. Phase-locked flow field measurements are used to identify wake structure. The measured tip vortex locations are compared with commonly used prescribed wake models.

Experimental Setup

Rotor System

The experiment was conducted on a three bladed rotor system, shown in Fig. 1, in a closed 6.4-by-7.0-by-4.9-m laboratory at the US Army Aeroflightdynamics Directorate. Two types of blades were used: (1) untwisted NACA 0012 blade that has a uniform chord of 0.060 m and a radius of 0.656 m, and (2) XV-15 *like* highly-twisted blade set that is made of 7 different airfoils, has a tip chord of 0.049 m, and has the same radius as that of the untwisted blade. Both the untwisted and twisted blades have 19% root cut out. More details of the scaled-down XV-15 blade can be obtained from Ref. 16.

The rotor system was equipped with a servo-motor that allowed the collective pitch adjustment of the rotor system on the fly. The torque sensor was placed behind the motor to measure the reaction torque. The thrust sensor was placed with the sensor axis coinciding with the axis of the rotor shaft.

Thrust and Torque Measurements

Performance measurements were made at several different rotational speeds, as well as at various collectives. The rotational speed, thrust and torque were all measured simultaneously for four seconds at a frequency of 1 KHz for each channel. The instantaneous measurements were averaged to estimate the mean and fluctuating values. The procedure was repeated ten times to estimate the repeatability. The repeatability was found to be within the instrument precision for both the thrust and torque measurements. The scatter was about 1% for both thrust and torque within the four second window. Thrust and torque tares were measured and subtracted.

Particle Image Velocimetry

Velocity field measurements were made across the entire span of both blade sets at five different thrust conditions corresponding to thrust coefficient (C_T) values of 0.00, 0.0013 (low thrust), 0.0028 (moderate thrust), and 0.0076 (high thrust). At the highest measured thrust of $C_T = 0.0083$, measurements were made only on the highly-twisted blades. All the PIV measurements for both blade sets were made at the rotational speed of 800 rpm corresponding to a tip speed of about 55 m/s.

The particle image velocimetry (PIV) system included dual Nd:YAG lasers that were operated in phase synchronization with the rotor, and an optical arm to transmit the laser light into the region of interrogation. A digital CCD

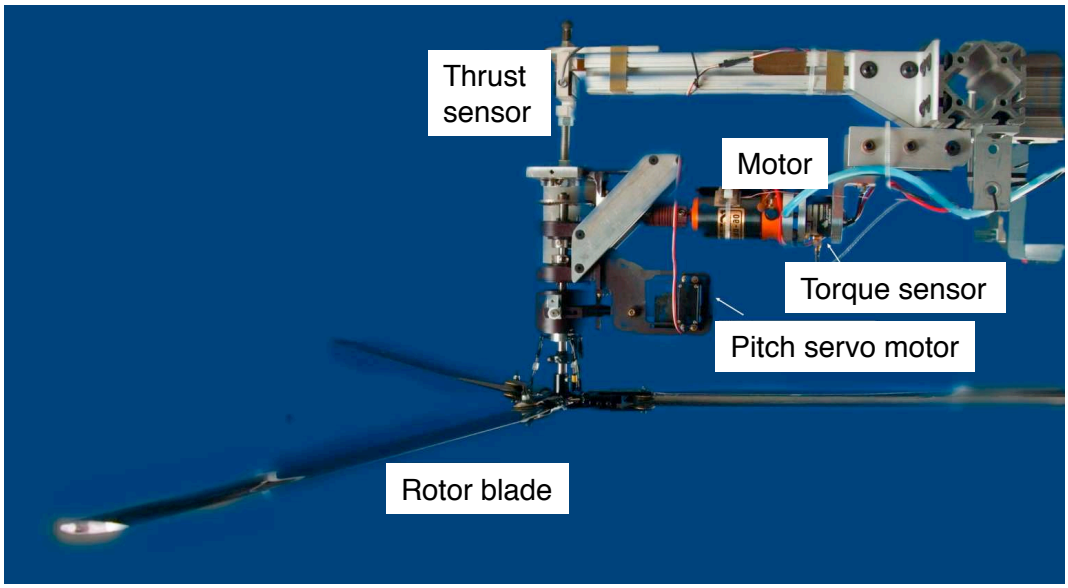

Figure 1: Close up view of the three-bladed rotor system.

camera with 11-megapixel resolution was placed normal to the laser light sheet, covering the entire span of the blade. A hall-effect switch was used to provide the 1/rev signal from the rotor to the laser for synchronization. The laser could be fired at any blade phase angle, enabling PIV measurements to be made at any wakeage. The two lasers were fired with a pulse separation time of 2-μs, which corresponded to less than 0.01° of blade azimuth.

The flow was seeded with a thermally produced mineral oil fog comprising particles approximately 0.2 microns in diameter; these were small enough to minimize particle tracking errors for the wake flows in these experiments (Ref. 17). The entire test area was uniformly seeded before each sequence of measurements.

In the present study, 100 images were acquired at each rotor azimuth relative to the PIV image plane. All the images were processed using an interrogation window of size 24-by-24 pixels with 50% overlap. A recursive technique called the deformation grid correlation (Ref. 18) was used as the correlation algorithm to process the PIV images. This is a better method for high-velocity gradient flows, such as those found inside rotor wakes. A detailed explanation of the recursive correlation technique, and other details of this correlation procedure are given in Ref. 19.

Results

This section describes the performance and flow field measurements of the highly-twisted and the untwisted blades. The rotor wake measurements are presented in both time- and phase-averaged form. The time-averaged measurements help relate the rotor to an actuator disk model, while the phase-averaged measurements help determine the vortical wake structure. Tip vortex trajectories obtained from the flow field are also presented along with classic prescribed wake predictions.

Performance Measurements

The performance of the highly-twisted blades is compared with that of the untwisted blades in Fig. 2, along with induced torque calculated using a simple blade-element momentum theory (BEMT) (Ref.20, pp. 87–113). The measured performance of both the untwisted blades and highly-twisted blades is identical. This suggests that the choice of twist is inconsequential at low Reynolds numbers, at least from a performance perspective. The highly-twisted blades are assumed to perform better than the untwisted blades because higher twist produces a more uniform inflow in the rotor disk plane. While this is certainly true at higher thrust coefficients, it is not so at lower thrust conditions, where most of the current measurements were performed. The BEMT induced torque calculations help understand this behavior. Notice that the untwisted blades show induced torque with the expected $\frac{{C_T}^{3/2}}{\sqrt{2}}$ trend, as shown in Fig. 2. The highly-twisted blades, in contrast, show a large induced torque at zero thrust. The benefits of twist are apparent for $C_T > 0.006$, where the highly-twisted blades yield a lower induced torque compared to the untwisted blades. However, the total torque does not show a similar benefit until the highest measured thrust. The flow field measurements shown later along with BEMT calculations for rotor inflow explain this key behavior.

Another interesting observation from Fig. 2 is that, despite yielding high induced torque at zero thrust, the total torque required by the highly-twisted blade remains at the

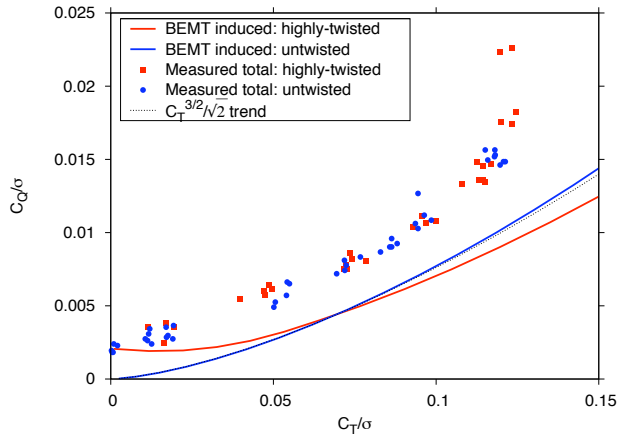

Figure 2: Induced torque calculated with BEMT compared with measured total torque

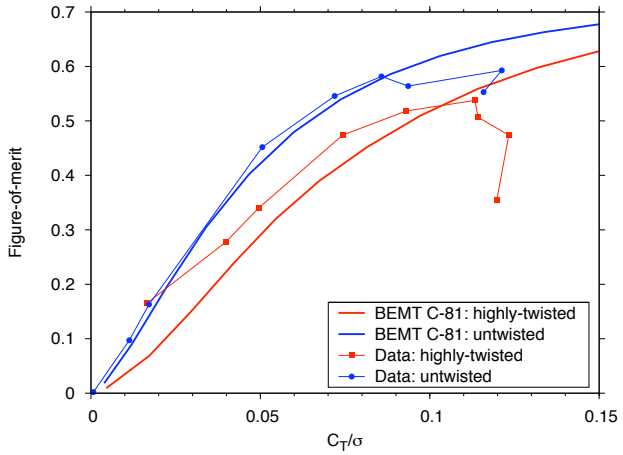

Figure 3: Figure of merit calculated with BEMT and C-81 table look-up for profile drag

same level as the untwisted blade. This means that the profile torque must be substantially lower for the highly-twisted blades than the untwisted blades, suggesting that the choice of airfoils at individual blade sections does indeed give significantly lower profile power as compared to the NACA 0012 airfoils.

In the present study, the improved performance associated with the twist was never realized because the blades began to stall due to the low tip Reynolds number. This is evident from Fig. 3 where the performance is shown in terms of figure of merit, i.e., the ratio of ideal induced power to the actual power. In this case only the measurements made at 800 RPM are shown. Also shown in Fig. 3 are the BEMT results for induced power that are supplemented with a simple C-81 table look-up for airfoil profile drag. For the highly-twisted blades the airfoil tables at low Reynolds number generated in Ref. 21 were used, while for the untwisted blades NACA 0012 airfoil tables were approximately corrected for Reynolds number effect by increasing the drag coefficient by 0.014, based on the results shown in Ref. 21.

The combined BEMT and C-81 drag look-up approach was not developed to provide accurate prediction of rotor performance, but merely to understand and explain the differences in the observed rotor performance. As seen in Fig. 3, the predicted trends very closely follow the measurements until blades experience stall. This good agreement may be partly fortuitous, but also demonstrates the importance of a simple theory for both prediction and understanding.

Flow Field Measurements

Representative flow field images acquired at 15 degree wakeage for both untwisted and highly-twisted blades are shown in Fig. 4. Corresponding PIV measurements are also shown. The overall differences in the wake characteristics between the two rotors at identical thrust ($C_T = 0.0076$) conditions are presented. Because both rotors have three blades, the adjacent tip vortices are 120 degrees apart. The tip vortices trailing highly-twisted blades diffuse faster than the vortices of untwisted blades, as expected. Another notable difference lies in the orientation of the inboard vortex sheets. For the highly-twisted blades, the sheets are almost parallel to the rotor disk plane. Because the vortex sheets convect at the local velocity, the sheet orientation is a reflection of relatively uniform inflow at these higher thrust conditions. On the other hand, for the untwisted blades, the outer edge of the wake sheet travels faster than the inner edges suggesting a linearly increasing inflow. The higher velocity near the tip of the blade is also reflected in the tip vortices for the untwisted blades, which travel downwards faster than those for the highly-twisted blades. Furthermore, the root vortices appear distinct in the case of highly-twisted blades. This may be because of the higher collective pitch at the root of the highly-twisted blades compared with the untwisted blades.

Similar phase-locked measurements were taken at 30 degree intervals (100 image pairs per wake age) and, were averaged at each phase angle for the phase-averaged results. Flow fields at all different phase angles were averaged together to obtain the time-averaged results.

Time-Average *vs*. **BEMT** The inflow distribution calculated using BEMT is compared with time-averaged inflow measurements in Fig. 5 at two thrust conditions. The measurements were performed by averaging time-averaged velocities at two planes just above and below the rotor disk plane. At $C_T = 0.0013$, the highly-twisted blades show large positive and negative velocities. The inboard portion produces a large downwash while the outboard portion produces a large upwash. This trend is also seen in the BEMT results. At the higher thrust condition ($C_T = 0.0076$), the highly-twisted blades give a somewhat uniform downwash which is also seen in the BEMT pre-

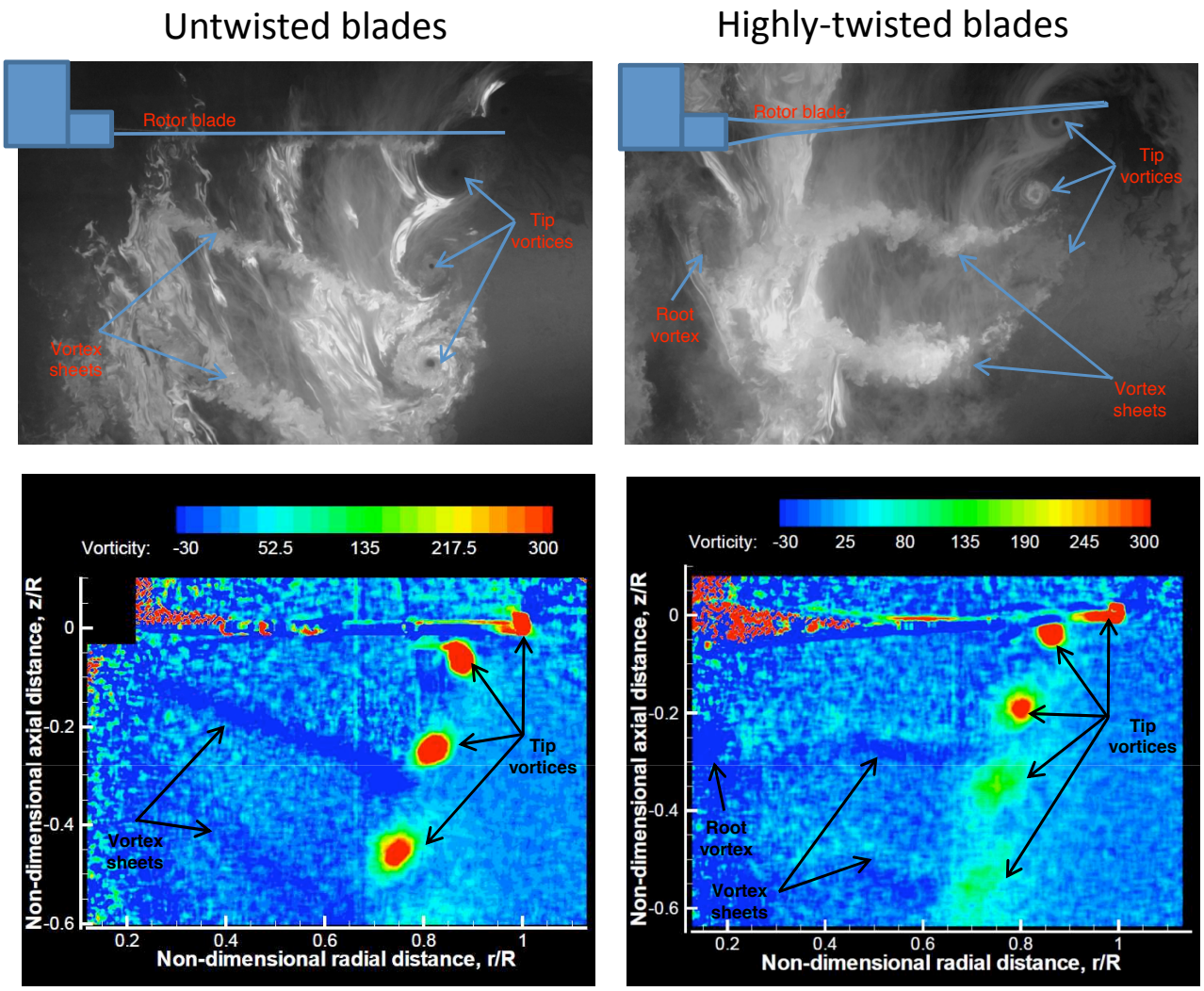

Figure 4: Laser light sheet flow visualization on untwisted and highly-twisted blades showing completely different wake characteristics

dictions. Untwisted blades, on the other hand, exhibit linear inflow distribution at both thrust conditions, and is correctly predicted by BEMT.

The BEMT inflow distribution corresponds to an actuator disk model while the measurements have discrete blades and trailing tip vortex effects, averaged over the rotor revolution. The measured inflow shows a sharp change in sign around 90%R leading to an upward velocity near the blade tip. Note that this is not the inflow seen by the blade, but rather it approximates the inflow for an actuator disk (infinite blades) by time-averaged inflow for a finite-bladed rotor. The rotor wake contracts radially and, as a result, there is an upward induced velocity outboard of the tip vortices. This leads to very little downwash or even a small upwash in the time-averaged velocities. The BEMT results do not show such upwash because they do not include the discrete blade tip vortices and wake contraction. However, the BEMT predictions show the same qualitative behavior as the measured data in both inflow distribution and rotor performance. The ability to predict this gross inflow distribution is key to the reasonably good performance predictions given by BEMT.

Time-Averaged Flow Field

Time-averaged flow field measurements are shown in Figs. 6 and 7. The left column shows the flow field of the highly-twisted blades while the right column shows the untwisted blades. Except for the zero thrust case, velocities are normalized using the ideal momentum theory uniform inflow velocity for the given thrust condition (i.e., $\sqrt{C_T/2}$).

The zero thrust condition shows the largest difference between the two blades. The untwisted blades produce no local lift and no downwash. However, the highly-

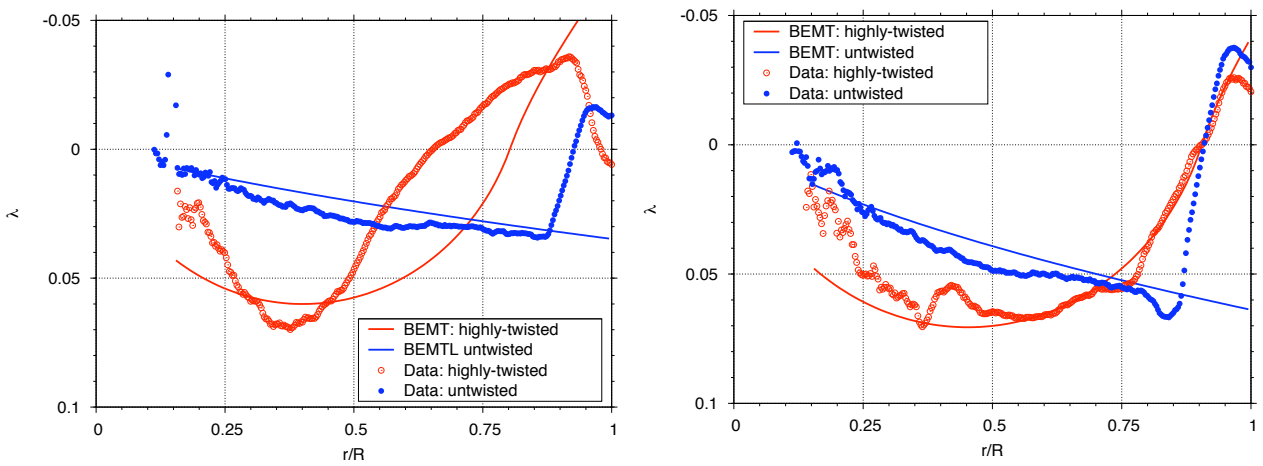

(a) C_T=0.0013 (b) C_T=0.0076

Figure 5: Averaged inflow at the rotor disk plane

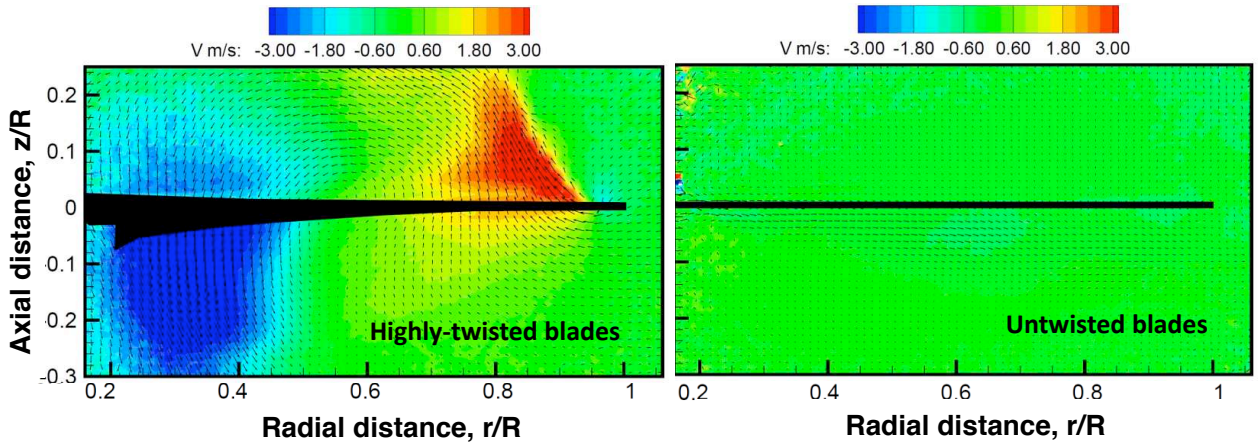

Figure 6: Time-averaged flowfield at zero thrust

twisted blades show a small region of somewhat uniform downwash near the blade root and a region of significant upwash near the tip. This, together with the large geometric twist, suggests that the inboard sections of the blade are producing positive lift while the outboard sections are producing negative lift. While the lift contributions of the individual blade sections cancel each other to give a net zero thrust, their induced drag contributions would be additive. This explains the large positive induced torque predicted by the BEMT analysis, as seen earlier in Fig. 2. At this thrust condition the flow field does not show any semblance of a contracting slipstream wake boundary below the rotor disk plane. Instead, there is a contracting slipstream boundary above the rotor near the tip. The flow is upward inside this slipstream boundary but then turns downwards flowing down through the rotor disk at inboard locations. Below the rotor disk there is non-contracting slipstream seen near 45%R that separates a region of almost uniform downwash inboard from quiescent flow outboard.

Figure 7 shows the time-averaged flow fields for the two rotors at $C_T = 0.0013$, 0.0028, and 0.0076. At $C_T = 0.0013$, the untwisted blades show linearly increasing downwash along the blade span. A contracting slipstream is clearly seen below the rotor separating a region of high downwash from outside quiescent flow. The flow field for the highly-twisted blades is similar to that at zero thrust but with an increased region of downwash over the inboard part of the blade. The region of upwash near the blade tip suggests that part of the blade may still be producing negative lift, but the overall thrust is positive because of positive lift on the inboard blade sections. The

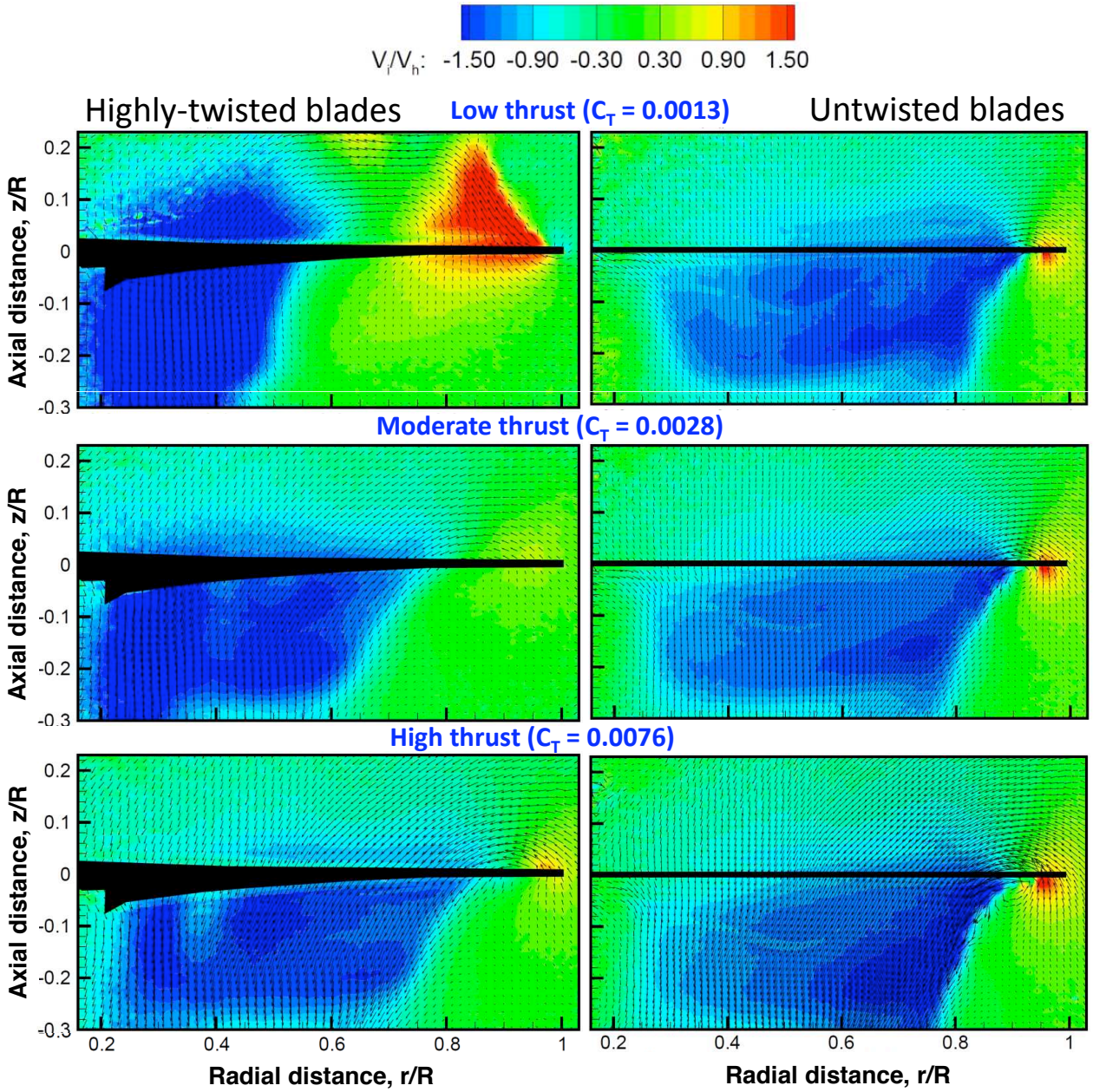

Figure 7: Time-averaged flowfield at higher thrust conditions

slipstream boundary is similar to that at zero thrust but is located further outboard at 50%R.

A further increase in thrust ($C_T = 0.0028$) does not seem to have much effect on the normalized downwash produced by the untwisted blades. The contour plots look essentially the same at different thrust conditions, suggesting that inflow distribution has the same shape with its magnitude increasing with rotor thrust coefficient. However, the flow field continues to change in the case of highly-twisted blades. At $C_T = 0.0028$, there is no upwash near the tip of the blade, suggesting that there is no negative thrust on any part of the blade. This is also likely because, at this thrust condition, the tip of the highly-twisted blade was at zero degree geometric pitch angle.

At $C_T = 0.0076$, the flow field for the untwisted blades continue to show the same trend as before, i.e., linear inflow distribution with increasing magnitude in downwash velocity with increasing C_T. The highly-twisted blades shows a more uniform inflow over most of the blade span, except near the blade tips. Also, the slipstream of the highly twisted blades appear to contract a little faster and a little further inboard compared to the untwisted blades.

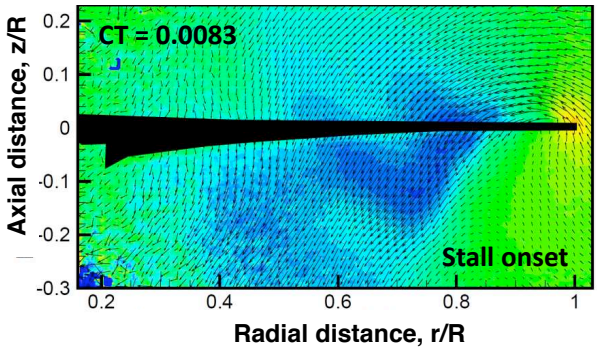

Figure 8: Time-averaged flowfield at stall for highly-twisted blade

Only the highly-twisted-blades were operated at the highest thrust of $C_T = 0.0083$. At this thrust condition, significant flow separation and stall occurred near the blade root, where the pitch angle is close to 50 degrees (see Fig. 8). The associated unsteadiness resulted in a relatively non-uniform flow field, more so near the root. Despite this flow separation, the rotor did produce higher thrust, albeit with a significant power penalty.

Phase-Averaged Flow Field

While the time-averaged flow field was useful to understand the overall rotor flow field, phase-averaged measurements were used to identify and understand the detailed flow features in the rotor wake. In this case, measurements were made with the PIV image plane "locked" at a given azimuth angle, ψ, relative to the rotor blade (phase). In Fig. 9, the highly-twisted blades are shown on the left with the untwisted blades on the right with all the measurements corresponding to 30 deg wake age. The images in Fig. 9 are sufficient to explain the flow physics, therefore measurements made at to other wake ages are not shown. Also, three of the six measured thrust conditions are shown here; $C_T = 0.0013$, low thrust condition; $C_T = 0.0028$, moderate thrust condition; and $C_T = 0.0076$, high thrust condition.

Figure 9 shows the flow field vorticity contours of both the rotors at the three thrust conditions. At least five key difference between the rotor flow fields are observed at the low thrust condition. First, the direction in which the tip vortices convect with respect to the rotor disk plane is different. Recall that the highly-twisted blades showed an upwash near the tip at this thrust condition. As a result, the tip vortices trailing from the highly-twisted blades convect upward and contract radially. On the other hand, the tip vortices trailing from the untwisted blades convect axially downward and radially inward. The second difference is rotation direction of the tip vortices. The untwisted blades show a counter-clockwise rotating tip vortex, while the highly-twisted blades show a clockwise rotating tip vortex. The third difference is the sign of vorticity in the vortex sheet. The untwisted blades have clockwise vorticity and highly twisted blades have counter clockwise vorticity. The fourth difference is the orientation/inclination of the vortex sheets with respect to the rotor disk plane. Lastly, there are subtle differences in the flow field near the blade root. The presence of clockwise rotating root vortices is visible for the highly-twisted blades. Root vortices are not evident for the untwisted blades, primarily because of the very small circulation, especially at low thrust conditions.

As thrust increases, the flow features such as the root vortex, vortex sheet and the tip vortices all remain identical (except for the natural increase in their strength) for untwisted blades. However, all these features seem to change with increasing thrust conditions for highly-twisted blades. These very different wake structures for the two blades reflect the underlying blade bound circulation distributions.

The schematic shown in Fig. 10 shows the circulation distribution that can be expected based on the inflow distribution, shown earlier in Fig. 6 and 7, at these three thrust conditions. In Fig. 10, the left column represents the flow field characteristics of highly-twisted blade, while the right column shows the flow characteristics of untwisted blades. In all cases, the root vortex corresponds to a large positive gradient in bound circulation corresponding to clockwise vorticity. The strength of the root vortices differs between the highly-twisted and untwisted blades. For highly-twisted blades, the bound circulation is larger near the root. Consequently, the root vortex would be strong even if the lift is lower because of the lower dynamic pressure. The root vortex trailing from the untwisted blades are much weaker in strength, and not visible at lower thrusts.

For the untwisted blades, the bound circulation linearly increases along the blade span leading to an inner wake sheet with clockwise vorticity. For the highly-twisted blades, the bound circulation decreases from the root to the tip essentially following the blade twist distribution. In this case, the inner wake sheet has counter-clockwise vorticity. The vorticity in the inner wake sheet has opposite sign for the untwisted and highly-twisted blades. This does not change with thrust. These observations are depicted in Figs. 10(a), (b) and (c) and verified through measurements shown in 9.

While the untwisted blades produce tip vortices that spin in the counter-clockwise direction at all thrust cases, the sign of the tip vortex changes with thrust for highly-twisted blades. At low thrust (e.g., $C_T = 0.0013$), recall that the outboard blade sections experience an upwash and produce negative lift. The corresponding bound circulation is also negative, resulting in clockwise vorticity in the tip vortices, see Figs. 9(a) and 10(a). At a slightly

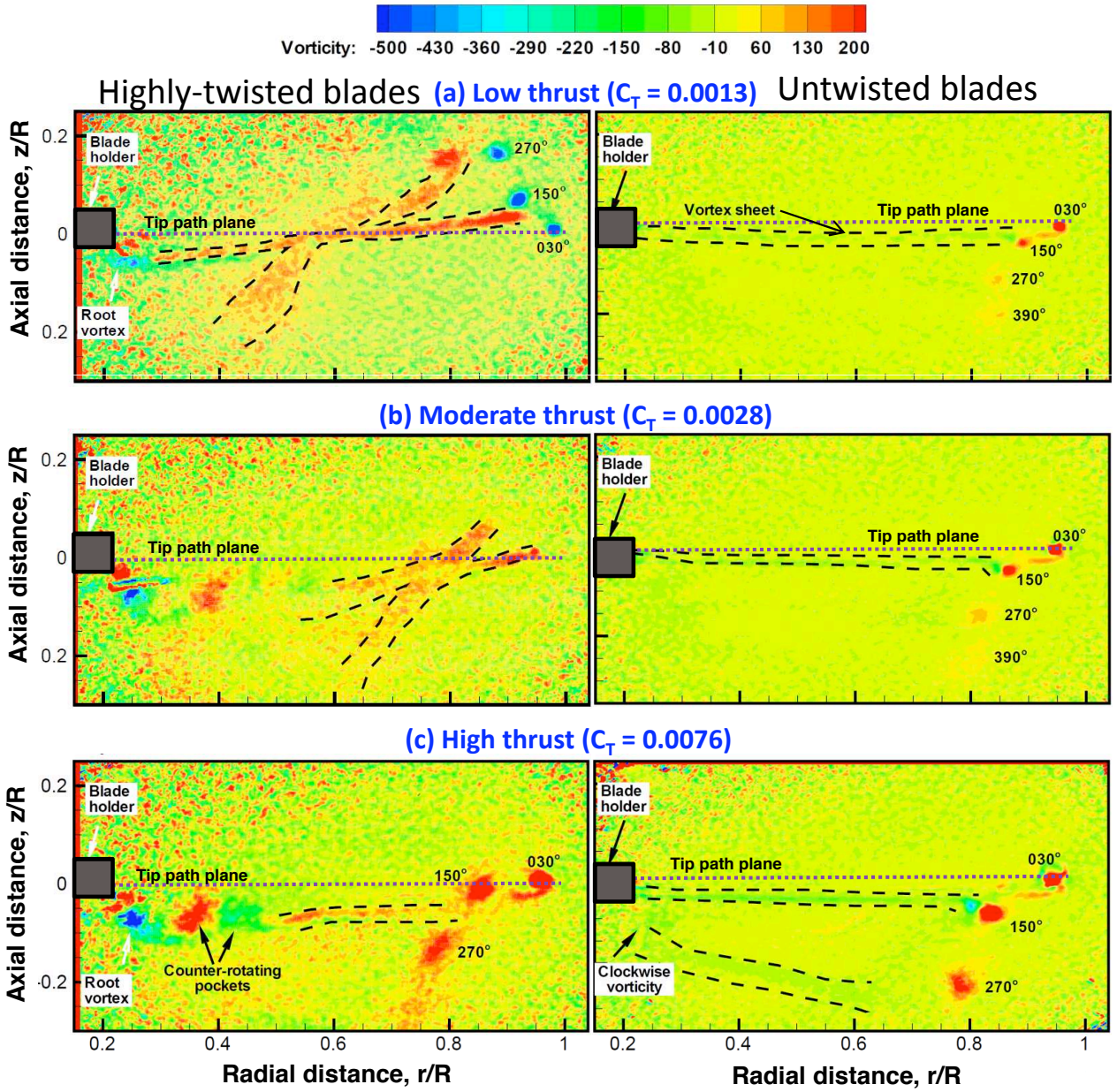

Figure 9: Phase-averaged flow fields shown as vorticity contours at three different thrust conditions

higher thrust, the blade tip operates at zero effective angle of attack and, in this case, there is no discernible tip vortex. This corresponds to Figs. 9(b) and 10(b). At even higher thrusts the blade tip region produces positive lift and, in turn, a positive bound circulation. Again, because the lift must vanish at the tip, the circulation must reduce resulting in a counter-clockwise tip vortex (Figs. 9(c) and 10(c)). Any further increase in thrusts would produce a similar wake structure with counter-clockwise vorticity in the tip vortices.

The inner wake sheet orientation shows the inflow distribution. For the untwisted blades, the inflow is linearly increasing along the blade span and this is clearly reflected in a nearly straight vortex sheet, with the outer edge convecting down faster than the inner edge. This observation is independent of the thrust condition – see Figs 9(a) to (c). On the other hand, the orientation of the vortex sheets changes with the thrust in the case of highly-twisted blades. At $C_T = 0.0013$, there is upwash near the tip and downwash near the root (see Fig. 6). Consequently, the outboard portion of the vortex sheets convects upward like the tip vortices (see Fig. 9(a)). The inboard edge of the

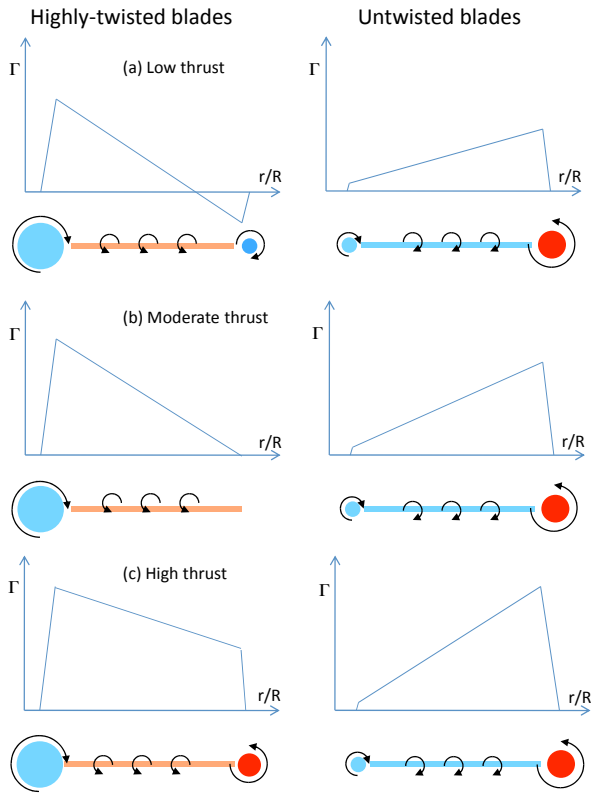

Figure 10: Schematic showing blade bound circulation and the resulting wake structure at different thrust conditions; (a) C_T=0.0013, (b) C_T=0.0028, and (c) C_T=0.0076.

vortex sheet convects downward resulting in sheets that appear to cross near 60%R. Figure 9(b) shows the flow fields at $C_T = 0.0028$. For the highly-twisted blades, no tip vortices are visible and the outer edge of the sheets continues to convect slowly upward and the sheets appear to intersect near 80%R. At $C_T = 0.0076$ (Fig. 9(c)), the inboard vortex sheets for the highly-twisted blades are almost parallel to the rotor disk plane and appear to convect faster than the tip vortices. This reaffirms the previous observation that inflow is nominally uniform at these high thrust conditions for the highly-twisted blades. The difference in inflow distribution between the two blades is reflected through the axial convection rate of the tip vortices trailing from both the blades. The tip vortices trailing from the untwisted blades travel downwards faster than those for the highly-twisted blades, as expected.

Tip Vortex Trajectory

Another piece of valuable information that can be gathered from the flow field is the tip vortex trajectory. The spatial locations of the tip vortices with respect to the blade tip were identified from the phase-locked, instantaneous velocity vector maps using local vorticity maxima as the criterion.

Measured tip vortex locations are shown in Fig. 11 at three different thrust conditions for both rotors along with the curve fits (explained in the following paragraph). The tip vortex trailing behind the untwisted blades travel axially downward from the rotor disk plane at all thrust conditions. The highly-twisted blades, however, showed varying behavior at different thrust conditions. At $C_T = 0.0013$, the tip vortices from the highly-twisted blades rapidly convect upward. At higher thrusts, when the entire blade may be producing positive thrust, the tip vortex initially convects upwards before beginning to convect downward after the first blade passage.

The well-known Landgrebe prescribed wake model (Ref. 2) describes the tip vortex trajectory parameters in terms of rotor thrust, solidity and linear twist rate. Another model is by Kocurek and Tangler (Ref. 14), where these parameters are described as a function of thrust coefficient, number of blades and linear twist rate. In both cases, the tip vortex geometry is described as a function of wake azimuth, ψ_w, in the generalized form

$$\frac{z}{R} = \begin{cases} k_1 \psi_w & 0 \le \psi_w \le \frac{2\pi}{N_b} \\ k_1 \frac{2\pi}{N_b} + k_2 \left(\psi_w - \frac{2\pi}{N_b}\right) & \psi_w \ge \frac{2\pi}{N_b} \end{cases} \quad (1)$$

$$\frac{r}{R} = A + (1-A)\exp(-\gamma\psi_w) \quad (2)$$

A radial contraction ratio, $A = 0.78$, is assumed for both models based on in a wide range of rotor wake experiments. The Landgrebe model gives the other parameters as

$$\begin{aligned} k_1 &= -0.25\left(\frac{C_T}{\sigma} + 0.001\theta_{tw}\right) \\ k_2 &= -(1.41 + 0.0141\theta_{tw})\sqrt{\frac{C_T}{2}} \\ \gamma &= 0.145 + 27C_T \end{aligned} \quad (3)$$

The Kocurek-Tangler model gives slightly different values for these parameters as

$$\begin{aligned} k_1 &= B + C\left(\frac{{C_T}^m}{{N_b}^n}\right) \\ k_2 &= -\sqrt{C_T - C_{T_0}} \end{aligned} \quad (4)$$

where

$$B = -0.000729\theta_{tw} \quad C = -2.30 + 0.206\theta_{tw} \quad C_{T_0} = {N_b}^n \left(\frac{-B}{C}\right)^{\frac{1}{m}}$$

$$m = 1.0 - 0.25\exp(0.040\theta_{tw}) \quad n = 0.5 - 0.0172\theta_{tw}$$

and the radial contraction rate is given by $\gamma = 4\sqrt{C_T}$.

The Landgrebe model also includes inboard vortex sheets described in terms of the displacements of their inner and outer edges. The Kocurek-Tangler model does

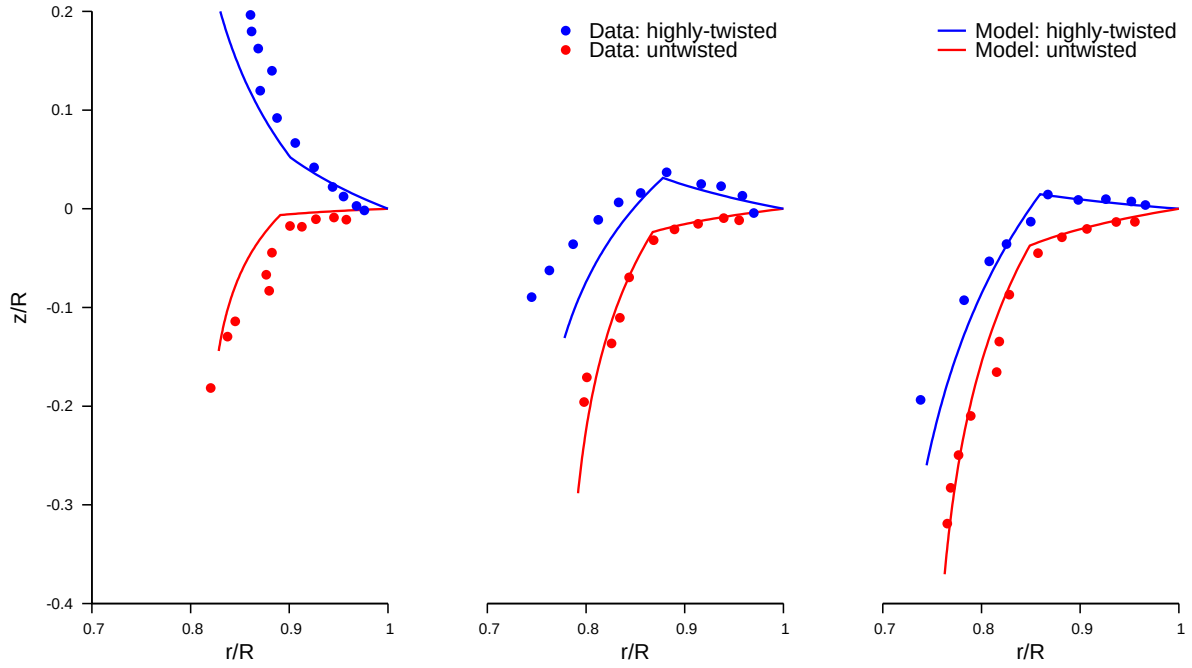

(a) $C_T = 0.0013$ (b) $C_T = 0.0048$ (c) $C_T = 0.0076$

Figure 11: Measured tip vortex locations and prescribed wake model

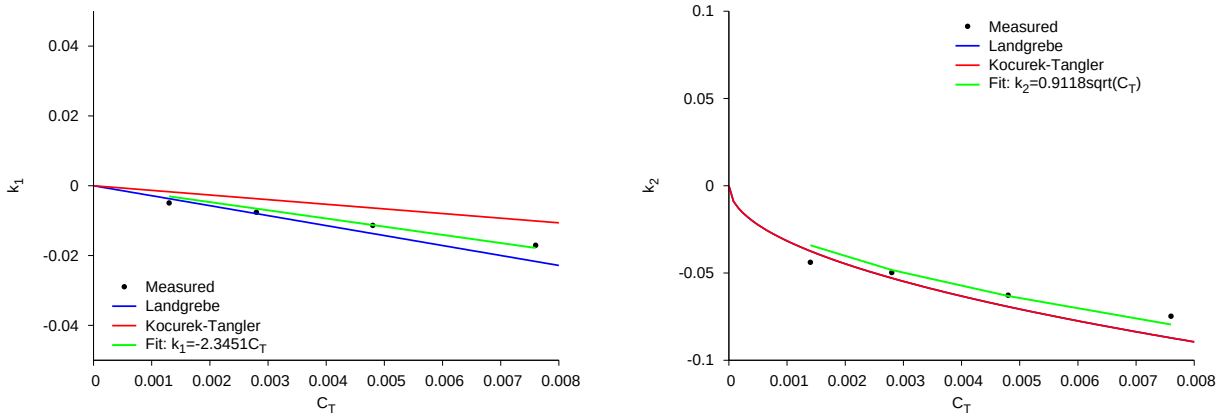

Figure 12: Axial convection rates for the untwisted blades

not explicitly include the inboard sheets. The observations made in the present study are similar to those found in the Landgrebe model in that the outer edge of the vortex sheet is seen to move much faster in the case of the untwisted blades than in the case of the highly-twisted blades.

Figures 12 and 13 show the axial tip vortex convection rates k_1 and k_2 estimated from the measured data using least-square fits. Landgrebe and Kocurek-Tangler models are also shown for comparison. For the untwisted blades, both models produced identical results and showed a relatively good correlation with the measurements. The highly-twisted blades are well outside the range of values used in forming these prescribed wake models. This can be understood from the poor predictions of the Landgrebe model, especially at low thrust conditions, when the tip vortices are traveling above the tip path plane. A curve fit is also shown using the same functional form as the Kocurek-Tangler model but with the coefficients being obtained by a least-square fit. The C_{T_0} parameter given by the Kocurek-Tangler model is too high. Other than that,

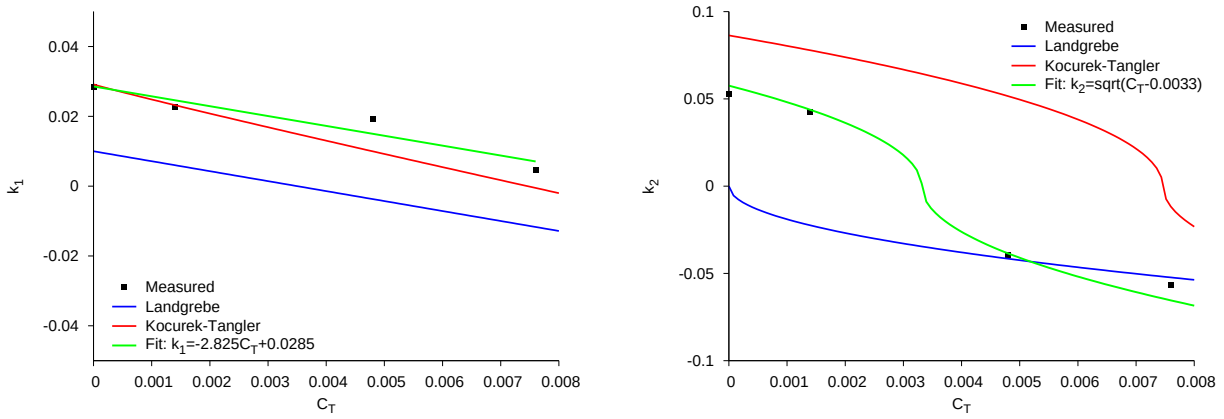

Figure 13: Axial convection rates for the highly-twisted blades

for the highly-twisted blades the Kocurek-Tangler model showed a very good agreement with the measured data. The radial contraction parameter γ also showed a similar trend, though not shown here.

Concluding Remarks

The present work reports performance and flow field measurements made on a three-bladed rotor with highly-twisted tilt-rotor like blades and untwisted blades. The experiments combined with a simple blade element momentum theory (BEMT) were used to understand the effect of twist on rotor performance and wake structure. The key observations and conclusions from the present study are enumerated below.

1. The performance with untwisted blades was as good as highly-twisted blades, if not marginally better. The highly-twisted blades yield improved performance because of lower induced power only at higher thrust coefficients. However, the model-scale highly twisted rotors were limited to low thrusts because of early on-set of blade stall at low Reynolds numbers.

2. BEMT calculations showed that at zero thrust the highly-twisted blades produced significant induced torque. However the measured torque at zero thrust was almost the same for both blades. This suggests that the XV-15 airfoils used on the highly-twisted rotor produced significantly lower profile drag as compared to the NACA 0012 airfoils used in the untwisted blades.

3. The untwisted blades produced similar flow fields at all thrusts, with a strong counter-clockwise tip vortex and a weaker inner wake sheet with clockwise vorticity. The steep orientation of the wake sheets indicated a linearly increasing inflow distribution along the blade span. A root vortex with clockwise vorticity was also observed at higher thrust conditions. The slipstream boundary below the rotor disk contracted to approximately 80%R.

4. The highly-twisted blades showed significant variation in inflow and wake structure at different thrust conditions. At lower thrust conditions, the observed inflow was not uniform. Instead, the inflow was higher near the blade root and decreased along the blade span toward the tip. This suggests that the lift and bound circulation also decreased from root to tip, resulting in an inner wake sheet with counter-clockwise vorticity. The high upwash near the blade tip suggests negative lift. This is confirmed by the observed strong tip vortices with clockwise vorticity. The tip vortex convected axially upwards while the root vortex convected downward. This resulted in very steep orientation of the inner wake sheets. The slipstream boundary below the rotor located close to mid-span, separating a large and approximately uniform downwash inboard from essentially quiescent flow outboard.

5. As rotor thrust increased on the highly-twisted blades, the upwash region was seen to decrease until it disappeared altogether at a certain moderate thrust condition. No discernible tip vortex was seen in the flow field. The wake structure comprising a root vortex with clockwise vorticity and inner wake sheet with counter-clockwise vorticity. The wake below the rotor disk contracted to about 60%R.

6. For the highly-twisted blades, at even higher thrusts, strong tip vortices with counter-clockwise vorticity were clearly evident, along with somewhat weaker inner wake sheets with counter-clockwise vorticity.

The slipstream below the rotor disk contracted to almost 71%R, and the initial contraction rate was faster as compared to the untwisted blades. The inner wake sheets were oriented almost horizontally indicating a uniform inflow distribution along the blade span. At such high thrust conditions, blade element momentum theory suggests that the highly-twisted blades would yield significantly lower induced power when compared to the untwisted blades. However, because of blade stall the measured rotor performance for the highly-twisted blades was no better than that of the untwisted blades.

Acknowledgements

The authors gratefully acknowledge the discussions with Drs. Wayne Johnson, Robert Ormiston, Frank Caradonna, and Mark Potsdam that were helpful throughout the work. The support of Mr. Perry Kavros in setting up the experiment was greatly appreciated.

References

[1]Gray, R. B., "An Aerodynamic Analysis of a Single-Bladed Rotor in Hovering and Low Speed Forward Flight As Determined From Smoke Studies of the Vorticity Distribution in the Wake," Aeronautical Engineering, Princeton University, 1956, no. 356.

[2]Landgrebe, A. J., "The Wake Geometry of a Hovering Rotor and its Influence on Rotor Performance," *Journal of the American Helicopter Society*, Vol. 17, No. 3, October 1972, pp. 3–15.

[3]Egolf, T. A., and Landgrebe, A. J., "Helicopter Rotor Wake Geometry and its Influence in Forward Flight, Vol. 1 — Generalized Wake Geometry and Wake Effects in Rotor Airloads and Performance," NASA CR-3726, October 1983.

[4]Lau, B. H., Wadcock, A. J., and Heineck, J. T., "Wake Visualization of a Full-Scale Tilt-Rotor in Hover," Proceedings of the AHS Technical Specialists' Meeting for Rotorcraft Acoustics and Aerodynamics, Williamsburg, VA, October 28–30, 1997.

[5]Yamauchi, G. K., Burley, C. L., Mercker, E., Pengel, K., and JanakiRam, R., "Flow Measurements of an Isolated Model Tilt Rotor," Proceedings of the American Helicopter Society 55th Annual National Forum, Montreal, Canada, May 25–27 1999.

[6]Biggers, J. C., Chu, S., and Orloff, K. L., "Laser Velocimeter Measurements of Rotor Blade Loads and Tip Vortex Rollup," Proceedings of the American Helicopter Society 31st Annual National Forum, Washington, D. C., May 13–15, 1975.

[7]Norman, T. R., and Light, J. S., "Rotor Tip Vortex Geometry Measurements Using the Wide-Field Shadowgraph Technique," *Journal of the American Helicopter Society*, Vol. 32, No. 2, April 1987, pp. 40–50.

[8]Komerath, N. M., Thomson, T. L., Kwon, O. J., and Gray, R. B., "Velocity Field of a Lifting Rotor Blade in Hover," *Journal of Aircraft*, Vol. 25, No. 3, March 1988, pp. 250–257.

[9]Caradonna, F., Hendley, E., Silva, M., Huang, S., Komerath, N., Reddy, U., Mahalingam, R., Funk, R., Wong, O., Ames, R., Darden, L., Villareal, L., and Gregory, J., "Performance Measurement and Wake Characteristics of a Model Rotor in Axial Flight," *Journal of the American Helicopter Society*, Vol. 44, No. 2, 1999, pp. 101–108 (Errata, Vol. 44, No. 3).

[10]Murashige, A., Tsuchihashi, A., Tsujiuchi, T., and Yamakawa, E., "Blade-Tip Vortex Measurement by PIV," Proceedings of the AHS Technical Specialists' Meeting for Rotorcraft Acoustics and Aerodynamics, Williamsburg, VA, October 28–30, 1997.

[11]Russel, J. W., Sankar, L. N., and Tung, C., "High Accuracy Studies of the Tip Vortex Structure from a Hovering Rotor," Proceedings of 28th AIAA Fluid Dynamics Conference and Exhibit, Snowmass Village, CO, June 29–July 2 1997.

[12]Heineck, J. T., Yamauchi, G. K., Wadcock, A. J., Lourenco, L., and Abrego, A. I., "Application of Three-Component PIV to a Hovering Rotor Wake," Proceedings of the American Helicopter Society 56th Annual National Forum, Virginia Beach, VA, May 2–4 2000.

[13]Ramasamy, M., Johnson, B., and Leishman, J. G., "Turbulent Tip Vortex Measurements Using Dual-Plane Stereoscopic Particle Image Velocimetry," *AIAA Journal*, Vol. 47, No. 8, July 2009, pp. 1826–1840.

[14]Kocurek, J. D., and Tangler, J. L., "A Prescribed Wake Lifting Surface Hover Performance Analysis," *Journal of the American Helicopter Society*, Vol. 22, No. 1, January 1977, pp. 24–35.

[15]Lorber, P. F., Stauter, R. C., Pollack, M. J., and Landgrebe, A. J., "A Comprehensive Hover Test of the Airloads and Airflow of an Extensively Instrumented Model Helicopter Rotor," Vol. 1-5, USAAVSCOM TR-D-16 (A-E), October 1991.

[16]McAlister, K. W., Tung, C., Rand, O., Khromov, V., and Wilson, J. S., "Experimental and Numerical Study of a Model Coaxial Rotor," Proceedings of the American Helicopter Society 62nd Annual National Forum, Phoenix, AZ, May 9–11 2006.

[17]Leishman, J. G., "On Seed Particle Dynamics in Tip Vortex Flows," *Journal of Aircraft*, Vol. 33, No. 4, July/August 1996, pp. 823–825.

[18]Scarano, F., "Iterative Image Deformation Methods in PIV," *Measurement Science and Technology*, Vol. 13, No. 1, 2002, pp. R1–R19.

[19]Ramasamy, M., and Leishman, J. G., "Benchmarking Particle Image Velocimetry with Laser Doppler Velocimetry for Rotor Wake Measurements," *AIAA Journal*, Vol. 45, No. 11, November 2007, pp. 2622–2633.

[20]Leishman, J. G., *Principles of Helicopter Aerodynamics,* Cambridge University Press, New York, 2000.

[21]Lim, J. W., McAlister, K. W., and Johnson, W., "Hover Performance Correlation for Full-Scale and Model-Scale Coaxial Rotors," *Journal of the American Helicopter Society*, Vol. 54, No. 3, July 2009.